Clim Dyn (2016) 46:1257–1276
DOI 10.1007/s00382-015-2643-9

NAO and PNA influences on winter temperature and precipitation over the eastern United States in CMIP5 GCMs

Liang Ning[1,2,3] · **Raymond S. Bradley**[2]

Received: 14 November 2014 / Accepted: 4 May 2015 / Published online: 24 July 2015

Abstract The historical and future relationships between two major patterns of large-scale climate variability, the North Atlantic Oscillation (NAO) and the Pacific/North America pattern (PNA), and the regional winter temperature and precipitation over the eastern United States were systemically evaluated by using 17 general circulation models (GCMs) from the Coupled Model Intercomparison Project phase 5. Empirical orthogonal function analysis was used to define the NAO and PNA. The observed spatial patterns of NAO and PNA can be reproduced by all the GCMs with slight differences in locations of the centers of action and their average magnitudes. For the correlations with regional winter temperature and precipitation over the eastern US, GCMs perform best in capturing the relationships between the NAO and winter temperature, and between the PNA and winter temperature and precipitation. The differences between the observed and simulated relationships are mainly due to displacements of the simulated NAO and PNA centers of action and differences in their magnitudes. In simulations of the future, both NAO and PNA magnitudes increase, with uncertainties related to the model response and emission scenarios. When assessing the influences of future NAO/PNA changes on regional winter temperature, it is found that the main factors are related to changes in the magnitude of the NAO Azores center and total NAO magnitude, and the longitude of the PNA center over northwestern North America, total PNA magnitude, and the magnitude of the PNA center over the southeastern US.

Keywords NAO · PNA · Teleconnection · CMIP5 · Regional climate

1 Introduction

According to the Intergovernmental Panel on Climate Change (IPCC) Fourth Assessment Report (AR4), global mean temperature shows a significant increase in recent decades, and precipitation has generally increased over land north of 30°N and decreased in the tropics, with substantial increases in heavy precipitation events and droughts in many continental regions (Trenberth et al. 2007). This conclusion has been confirmed by previous studies for different regions (e.g. Ning and Qian 2009; Kunkel et al. 2013). For example, Hartmann et al. (2013) found that there have been increases in either the frequency or intensity of heavy precipitation over the United States since about 1950. Based on general circulation model (GCM) simulations, Meehl et al. (2007) concluded that warming would very likely continue, with increased precipitation extremes and droughts.

The North Atlantic Oscillation (NAO; Wallace and Gutzler 1981; Barnston and Livezey 1987), and Pacific-North

Electronic supplementary material The online version of this article (doi:10.1007/s00382-015-2643-9) contains supplementary material, which is available to authorized users.

✉ Liang Ning
lning@geo.umass.edu

[1] Key Laboratory of Virtual Geographic Environment of Ministry of Education, School of Geography Science, Jiangsu Key Laboratory for Numerical Simulation of Large Scale Complex System, School of Mathematical Science, Nanjing Normal University, Nanjing 210023, China

[2] Department of Geosciences, Northeast Climate Science Center, Climate System Research Center, University of Massachusetts, Amherst, MA 01003, USA

[3] Jiangsu Center for Collaborative Innovation in Geographical Information Resource Development and Application, Nanjing 210023, China

American pattern (PNA; Wallace and Gutzler 1981; Leathers et al. 1991) are two major modes of large-scale climate variability that have large-scale effects on precipitation and temperature patterns. The NAO reflects the fluctuations of the sea level pressure (SLP) difference between the Icelandic Low and the Azores High. During the positive phase, the SLP difference is larger than the normal condition, and vice versa. The PNA reflects the quadripole pattern of the 500 hPa geopotential height (H500) anomaly field, with action centers over the vicinity of Hawaii, the Aleutian Islands, northwestern North America, and the southeastern US During the positive PNA phase, there are above-average H500 over the vicinity of Hawaii and northwestern North America, and below-average H500 over the Aleutian Islands and the southeastern US, and vice versa. Both NAO and PNA have strong influences on regional climate over the eastern US (Hartley and Keables 1998; Bradbury et al. 2003; Ning et al. 2012b). For example, when investigating the impacts of NAO on Great Lakes ice cover, Bai et al. (2012) found that the Great Lakes tend to have lower ice cover during years with a positive NAO, and vice versa. Coleman and Rogers (2003) showed that the PNA has significant negative correlations with winter precipitation over the Ohio River Valley, as during negative PNA winters, moisture flux convergence extends much farther north from the Gulf of Mexico and brings more precipitation. Ge et al. (2009) pointed out that the PNA also influences snow conditions over portions of North America through its influence on both winter temperature and precipitation.

GCMs based on well-established physical principles reproduce observed features of recent climate (Randall et al. 2007), and they are the major tools used to project future climate, including both large-scale climate variability patterns and regional temperature and precipitation extremes (Meehl et al. 2007). GCM outputs have also been used in studies of climate influences on water resources, environment, and ecosystems through different downscaling methods (e.g. Hewitson and Crane 1996, 2006; Ning et al. 2012a). GCMs in the Coupled Model Intercomparison Project phase 5 (CMIP5) archive use both new parameterization schemes and new Representative Concentration Pathway (RCP) scenarios, which provide more plausible descriptions of how the future socioeconomic, technological and environmental conditions, and associated emissions of greenhouse gases and aerosols may develop (Moss et al. 2010; Taylor et al. 2012).

The abilities of multi-model simulations in CMIP3 and CMIP5 to reproduce the NAO and PNA characteristics have already been assessed in previous literature (Casado and Pastor 2012; Stoner et al. 2009; Lee and Black 2013; Davini and Cagnazzo 2014). In this study, we evaluate the GCMs' performances on simulations of the relationships between NAO/PNA and regional winter climate over the eastern US, and the corresponding uncertainties in future projections. This assessment is an important step before applying CMIP5 GCM output to regional climate projections over the eastern US This region encompasses enormous diversity in geography, climate, ecological resources, and human land use with a human population of 131 M (41 % of the US population). Consequently, the eastern US region poses many unique challenges for understanding, adapting to, and mitigating the effects of climate change on the environment, particularly water resources, and ecosystems (Horton et al. 2014).

2 Data and methodology

2.1 Data

The winter season (DJFM) SLP and H500 field from the National Centers for Environmental Prediction (NCEP) reanalysis data (Kalnay et al. 1996) for the period 1950–1999 are used to define the observed NAO and PNA. The reason that March is included in this study is that previous studies have shown that winter conditions usually persist until March over the northeastern US, especially in the New England region (e.g. Kunkel and Angel 1999; Bradbury et al. 2003).

The GCM winter monthly temperature, precipitation, SLP, and H500 data for the periods 1950–1999 and 2050–2099 are taken from the World Climate Research Programme (WCRP) CMIP5 simulations for the historical emission scenario and future RCP2.6, RCP4.5, and RCP8.5 scenarios (Moss et al. 2010; Taylor et al. 2012), for 17 different models (Table 1). These three RCP scenarios range from low to high-emissions, and are defined on the basis of year 2100 radiative forcing values, e.g. 2.6 W/m^2 in RCP2.6 scenario and 8.5 W/m^2 in RCP8.5 scenario (van Vuuren et al. 2011). The data and detailed descriptions of the GCMs can be found at the Program for Climate Model Diagnosis and Intercomparison (PCMDI) website http://pcmdi9.llnl.gov/esgf-web-fe/.

For our analysis, we focus on the eastern US (24–50°N and 100–68°W). The University of East Anglia Climatic Research Unit (CRU) TS3.21 high-resolution (0.5°) observed winter monthly temperature and precipitation data used in this study are for the period 1950–1999 (Harris et al. 2014). The observed NAO and PNA time series from National Center for Atmospheric Research (NCAR) and National Oceanic and Atmospheric Administration (NOAA) are also used for validations of the NAO and PNA time series generated from NCEP data in this study.

2.2 Methodology

To define the NAO and PNA indices, there are usually two methods used. One method is to linearly composite

Table 1 The CMIP5 GCMs used in this study

	Model	Institution	References
1	CanESM2	Canadian Centre for Climate Modelling and Analysis, Canada	Chylek et al. (2011)
2	CCSM4	National Center for Atmospheric Research (NCAR), USA	Gent et al. (2011)
3	CESM1-CAM5	NSF/DOE NCAR, USA	Neale et al. (2013)
4	CESM1-WACCM	NSF/DOE NCAR, USA	Liu et al. (2010)
5	CNRM-CM5	Centre National de Recherches Meteorologiques, Meteo-France, France	Voldoire et al. (2012)
6	CSIRO-MK3.6.0	Australian Commonwealth Scientific and Industrial Research Organization, Australia	Rotsayn et al. (2010)
7	FGOALS-g2	Institute of Atmospheric Physics, Chinese Academy of Sciences, China	Zhou et al. (2013)
8	GFDL-CM3	NOAA Geophysical Fluid Dynamics Laboratory (GFDL), USA	Donner et al. (2011)
9	GISS-E2-H	NASA Goddard Institute for Space Studies (GISS), USA	Schmidt et al. (2014)
10	HadGEM2-AO	Met Office Hadley Centre, UK	Johns et al. (2006)
11	HadGEM2-ES	Met Office Hadley Centre, UK	Bellouin et al. (2007) and Collins et al. (2008)
12	IPSL-CM5A-MR	Institut Pierre-Simon Laplace, France	Mignot and Bony (2013)
13	MPI-ESM-LR	Max Planck Institute for Meteorology, Germany	Raddatz et al. (2007) and Marsland et al. (2003)
14	MPI-ESM-MR	Max Planck Institute for Meteorology, Germany	Raddatz et al. (2007) and Marsland et al. (2003)
15	MRI-CGCM3	Meteorological Research Institute, Japan	Yukimoto et al. (2011)
16	MIROC5	Atmosphere and Ocean Research Institute (AORI), (National Institute for Environmental Studies), JAMSTEC (Japan Agency for Marine-Earth Science and Technology), Japan	Watanabe et al. (2010)
17	NorESM1-M	Norwegian Climate Centre, Norway	Bentsen et al. (2012)

the normalized SLP and H500 anomalies at specified grid points corresponding to "centers of action" or antinodes of the patterns (e.g. Wallace and Gutzler 1981; Hurrell 1995). Another method is to use empirical orthogonal functions (EOFs) to extract the major patterns from the entire SLP and H500 field over the northern hemisphere (e.g. Barnston and Livezey 1987; Hurrell and Deser 2009; Allan et al. 2014). The major advantage of the linear composition method is that it can directly show the magnitudes of teleconnections. Compared to the linear composition method, EOF analysis can capture the spatial variability of the action centers, although it requires a larger spatial domain for the analysis. In this study, we use both methods, and apply them to different analyses to take full advantage of the two methods.

3 Results

3.1 Spatial patterns

To evaluate the simulations of the influences on winter climate over the eastern US, the spatial patterns of the simulated NAO and PNA are first compared with the observed data. Figure 1 shows the regression patterns of the first EOF mode on SLP anomalies from the NCEP data and 17 GCMs for the period 1950–1999. Because the NAO patterns are shown in the first EOF mode, and the "unphysical pattern issue" that results from the orthogonality constraint of EOF analysis does not influence the results (cf. Hannachi 2007; Lian and Chen 2012), no additional rotation of EOF is applied here. The correlation coefficient between the observed NAO index (defined here as the time series of the first EOF), and the observed NAO index defined using the difference of normalized SLP between Lisbon, Portugal and Stykkishomur/Reykjavik, Iceland (Hurrell et al. 2013) is 0.99 ($p < 0.01$). All the GCMs can reproduce an obvious dipole consisting of a high over the Azores and a low over Iceland, which is the characteristic feature of the NAO. For the NCEP data (Fig. 1a), the first pattern explains 54.1 % of the total variance, while for GCMs (Fig. 1b–r), the variances explained by the first patterns are about 50 % for most GCMs, with the smallest two (37.2 and 37.6 %) from HadGEM2-AO (Fig. 1k) and HadGEM2-ES (Fig. 1l). For the locations of NAO centers, most GCMs can reproduce this quite well, though several [CNRM-CM5 (Fig. 1f), CSIRO-Mk3.6.0 (Fig. 1g), FGOALS-g2 (Fig. 1h), GISS-E2-H (Fig. 1j), and MIROC5 (Fig. 1q)] simulate the NAO positive centers as extending too far to the west. Most GCMs underestimate the magnitude of NAO positive centers, while three overestimate the magnitude [CSIRO-Mk3.6.0 (Fig. 1g), IPSL-CM5A-MR (Fig. 1m), and MIROC5 (Fig. 1q)]. Most simulated magnitudes of NAO negative centers are close to the observations [with only CNRM-CM5 (Fig. 1f), CSIRO-Mk3.6.0

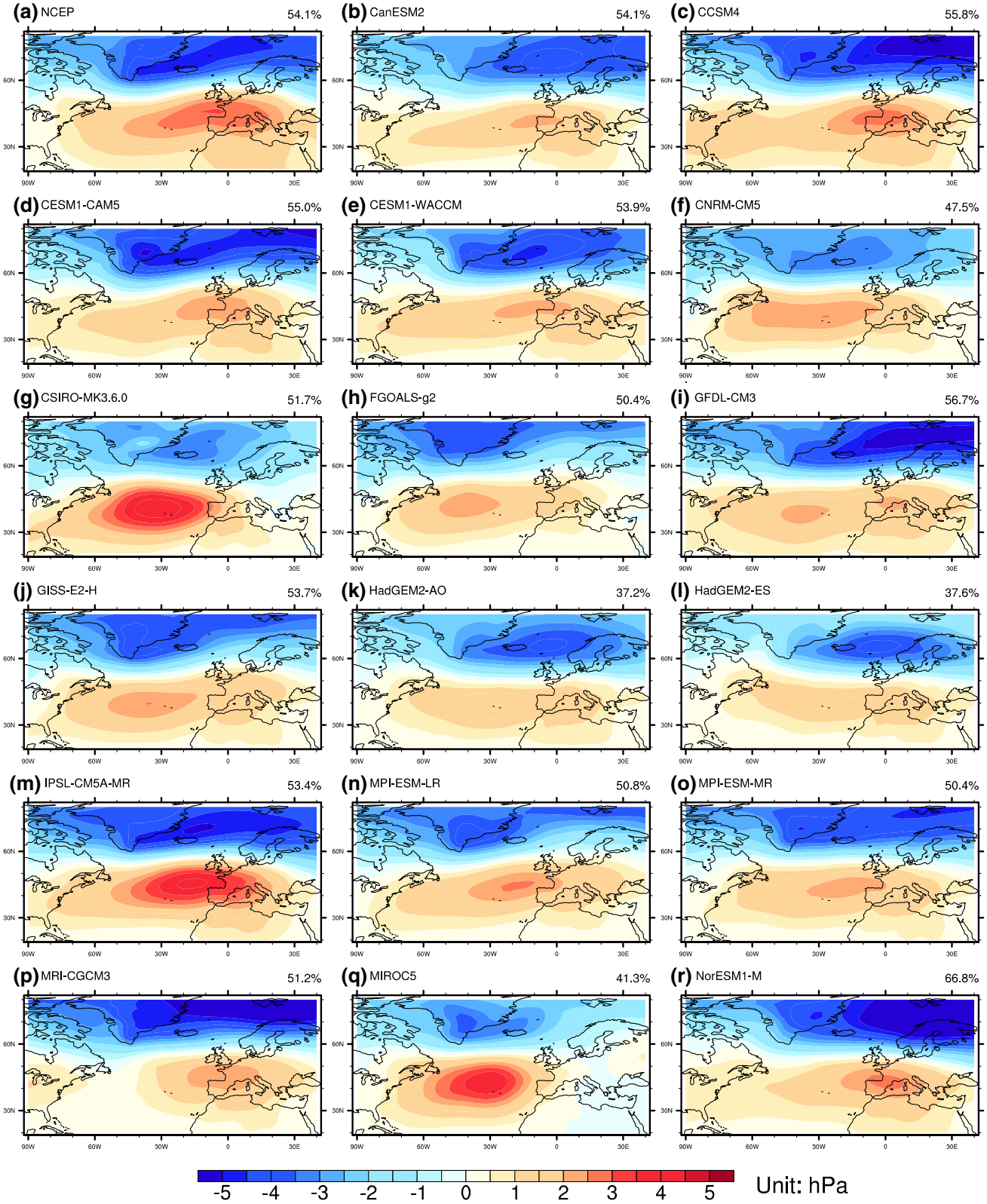

Fig. 1 The spatial regression patterns of the first EOF mode on the SLP pressure anomalies from observations (NCEP) (*upper left panel*) and 17 GCMs (unit: hPa)

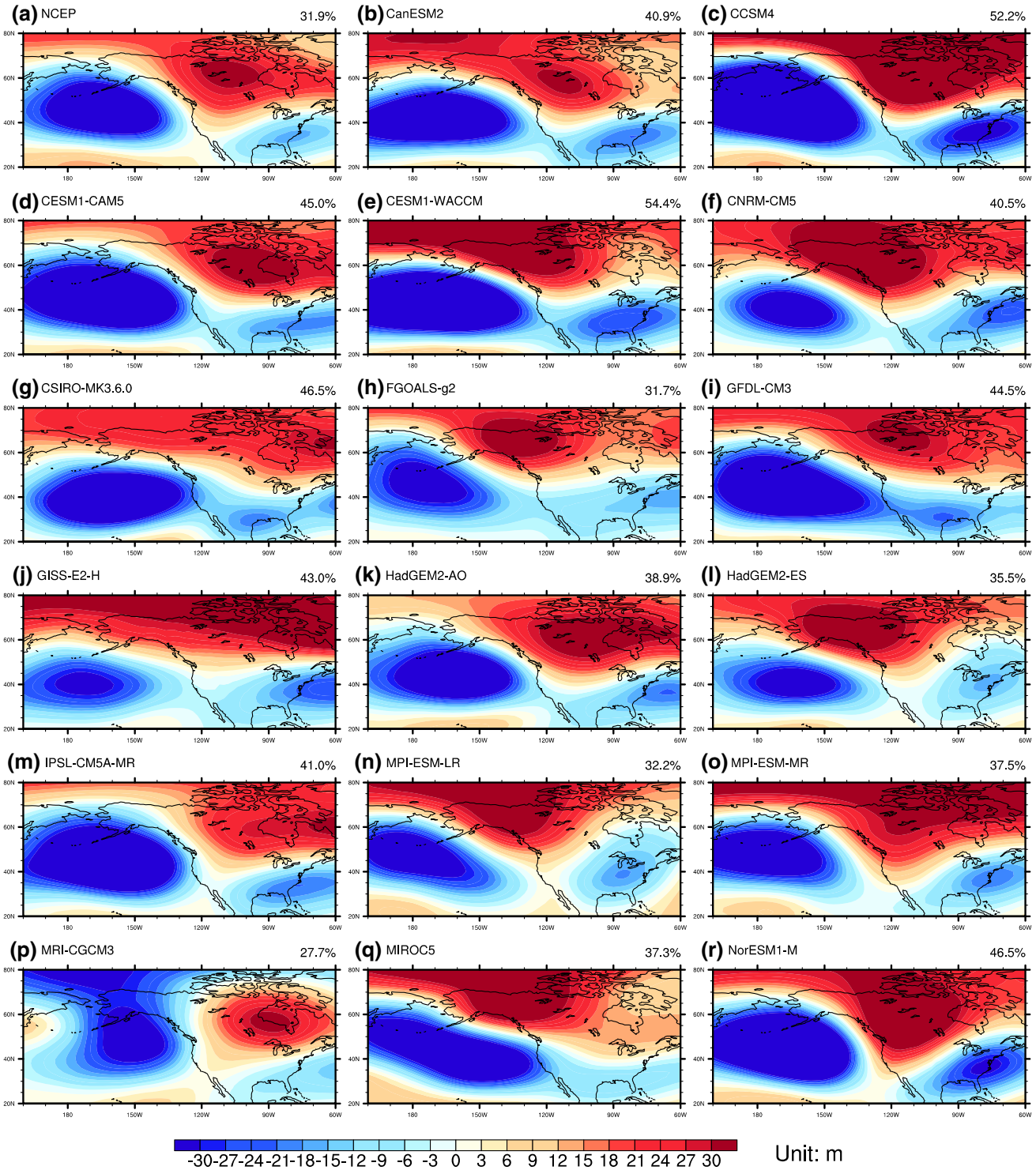

Fig. 2 The spatial regression patterns of the first EOF mode on the H500 anomalies from the observations (NCEP) (*upper left panel*) and 17 GCMs (unit: m)

(Fig. 1g), HadGEM2-ES (Fig. 1l), and MIROC5 (Fig. 1q) slightly underestimating the magnitude].

Figure 2 shows the regression patterns of the first EOF mode on H500 anomalies from the NCEP data and 17 GCMs for the period 1950–1999. In this study, since we mainly focus on the climatic influences over the eastern US, the region used to define PNA is 30–50°N, 160°E–60°W, which contains three of the four action centers that have the

largest influences over the eastern US (Allan et al. 2014). Using NCEP data (Fig. 2a), the three centers of action (located over the Aleutian Islands, northwestern North America, and the southeastern US) are well captured by the EOF analysis, with 31.9 % variance explained by the first EOF. The time series of the first EOF is also highly correlated with the PNA index defined using the difference of the normalized H500 field ($r = 0.91$, $p < 0.01$). In all of the GCM simulations, these three centers are reproduced, with ~40 % variance explained (Fig. 2b–r). Among the three centers, usually the locations of the negative height centers over the Aleutian Islands and the southeastern US can be reproduced correctly with small differences (e.g. CNRM-CM5, Fig. 2f; HadGEM2-ES, Fig. 2l; MPI-ESM-LR, Fig. 2n; MRI-CGCM3, Fig. 2p), while the positive height centers over northwestern North America are displaced in several GCM simulations (e.g. GFDL-CM3, Fig. 2i; GISS-E2-H, Fig. 2j; MRI-CGCM3, Fig. 2p). The magnitudes of the negative height centers over the Aleutian Islands and positive height centers over northwestern North America are usually simulated reasonably, while the magnitudes of the negative height centers over the southeastern US are overestimated in several GCMs [e.g. CCSM4 (Fig. 2c), CESM1-WACCM (Fig. 2e), CNRM-CM5 (Fig. 2f), and GISS-E2-H (Fig. 2j), and NorESM1-M (Fig. 2r)].

From the analysis of this section, it can be concluded that the spatial patterns of the NAO and PNA can be reproduced reasonably by most of the CMIP5 GCMs, similar to the performances of those models included in the CMIP2 archives (Stephenson et al. 2006) and CMIP3 archives (Handorf and Dethloff 2012). To quantitatively evaluate the GCMs' performance in reproducing the spatial patterns, the spatial correlations between the observed and simulated NAO/PNA patterns are calculated after being regridded to the same 2° × 2° resolution (Table 2). From the table, it can be seen that the observed NAO pattern is usually well reproduced by the GCMs, with an average correlation coefficient of 0.94. The lowest coefficients are from CSIRO-Mk3.6.0 ($r = 0.87$) and MIROC5 ($r = 0.83$), which underestimate the negative centers but overestimate the positive centers and displace the positive centers towards the middle of the Atlantic Ocean. All these correlation coefficients are skillful when using a reference value of 0.6 as an evaluation limit (Hollingsworth et al. 1980; Wilks 2006). The GCMs have less skill in reproducing the PNA patterns, with an average correlation coefficient of 0.85. The five GCMs with coefficients lower than 0.8, i.e. CNRM-CM5 ($r = 0.74$), GISS-E2-H ($r = 0.74$), HadGEM2-ES ($r = 0.74$), MPI-ESM-LR ($r = 0.75$), and MRI-CGCM3 ($r = 0.48$, which is the only correlation coefficient lower than reference value 0.6), usually simulate some displacements of the three centers, and differences in magnitudes.

Table 2 The spatial correlations between observed and simulated NAO and PNA patterns in CMIP5 GCMs

	Model	NAO	PNA
1	CanESM2	0.96	0.90
2	CCSM4	0.97	0.96
3	CESM1-CAM5	0.98	0.96
4	CESM1-WACCM	0.98	0.88
5	CNRM-CM5	0.96	0.74
6	CSIRO-MK3.6.0	0.87	0.82
7	FGOALS-g2	0.93	0.84
8	GFDL-CM3	0.97	0.93
9	GISS-E2-H	0.97	0.74
10	HadGEM2-AO	0.93	0.97
11	HadGEM2-ES	0.88	0.74
12	IPSL-CM5A-MR	0.98	0.93
13	MPI-ESM-LR	0.96	0.75
14	MPI-ESM-MR	0.97	0.90
15	MRI-CGCM3	0.94	0.48[a]
16	MIROC5	0.83	0.86
17	NorESM1-M	0.94	0.97
	Average	0.94	0.85

[a] Not significant

3.2 Relationships with regional temperature and precipitation

After evaluating the simulated spatial patterns of NAO and PNA, the GCMs' performances in reproducing the observed relationships between NAO/PNA and regional winter climate over the eastern US were investigated.

From observations, the NAO has a significant positive correlation ($p = 0.05$) with winter average temperature (0.5° resolution) over most parts of the eastern US (Fig. 3a). The probable mechanism is that the positive pressure anomalies induce a weaker H500 trough over the eastern US and block polar air invasion into this region during positive NAO winters (Ning and Bradley 2015). All GCMs can reproduce this positive correlation between the simulated NAO index and simulated temperature, while several GCMs simulate a smaller region with significant positive correlations, due to underestimation of the NAO positive center magnitudes, and extension over the eastern US, [e.g. CanESM2 (Fig. 3b), CESM1-CAM5 (Fig. 3d), HadGEM2-AO (Fig. 3k), HadGEM2-ES (Fig. 3l), and NorESM1-M (Fig. 3r)]. On the other hand, CSIRO-Mk3.6.0 (Fig. 3g) and MIROC5 (Fig. 3q), which overestimate the NAO magnitudes and the western extension, simulate more robust significant positive correlations.

For winter precipitation, based on the observations, NAO has a positive correlation with precipitation over the

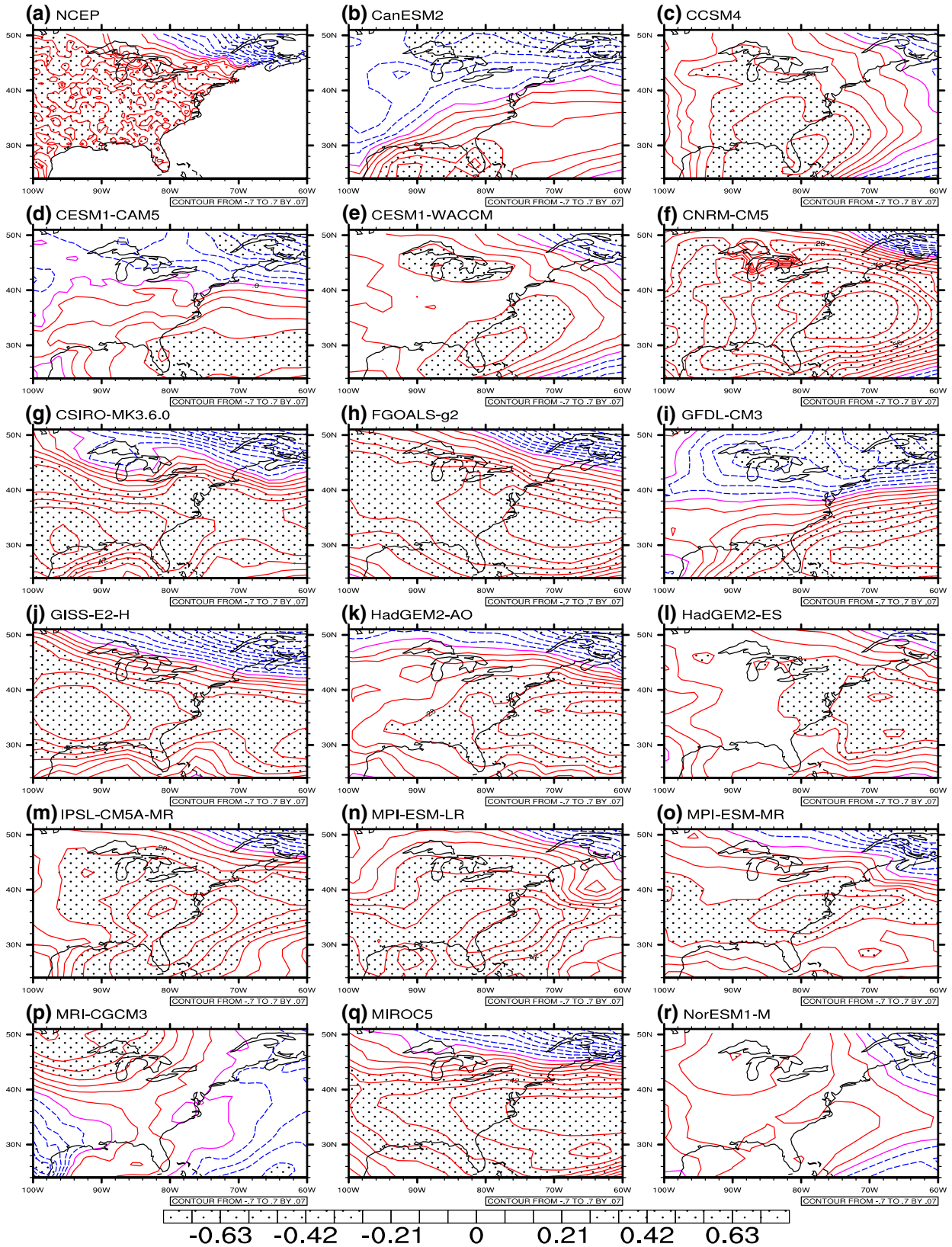

Fig. 3 The observed and GCM simulated correlations between the NAO and regional winter temperature over the eastern US (contour interval 0.07). *Red solid lines* indicate positive correlations. *Blue dash lines* indicate negative correlations. *Stippling* indicates correlations significant at the $p = 0.05$ level

southeastern US with significant correlations only over a small region in the south, and a slightly negative correlation along the coast of New England and into Maine (Fig. 4a) (c.f. Bradbury et al. 2003). Since the precipitation correlation pattern is more spatially heterogeneous, the contour interval shown is larger than the temperature correlation, to make the pattern clearer. This pattern is captured to some extent by several GCMs, but with some displacement of the centers and differences in magnitudes, due to differences between the observed and simulated NAO extensions and magnitudes [e.g. CanESM2 (Fig. 4b), CCSM4 (Fig. 4c), CNRM-CM5 (Fig. 4f), and GISS-E2-H (Fig. 4j)]. FGOALS-g2 (Fig. 4h), MPI-ESM-LR (Fig. 4n), and MIROC5 (Fig. 4q) simulate positive correlations over the whole eastern US, but for other GCMs, the simulated patterns are quite different from the observations. For example, in GFDL-CM3 (Fig. 4i), the simulated NAO has a negative correlation with winter precipitation over the whole region. The potential reason is the simulated NAO extends too far to the west, and the positive pressure anomalies (Fig. S1a) block the winter storms, so that there is less precipitation during positive NAO winters (Fig. S1b).

Figure 5 compares the observed and GCM-simulated spatial patterns of the correlations between the PNA index and winter temperature over the eastern US The observed PNA index has a positive correlation with winter temperature over the northwest part of the region and a negative correlation to the southeast. The mechanism is that the positive geopotential height anomaly over northwestern North America and negative geopotential height anomaly over the southeastern US displace the polar jet stream to the southeast, inducing a deeper trough over the eastern US (Notaro et al. 2006), which leads to the advection of northerly air into the southeastern part of the region, resulting in negative temperature anomalies. By contrast, the positive geopotential height anomalies over northwestern North America induce poleward displacement of the polar jet over the western US, and this enhanced ridge brings positive temperature anomalies over the region dominated by positive geopotential height anomalies, including the northwestern part of the study region (Ning and Bradley 2015). All of the GCMs can generally reproduce this northwest-southeast contrast pattern, though with some differences in the locations of the boundary between positive and negative correlations. Within the GCMs, several GCMs can reproduce quite similar patterns, e.g. CanESM2 (Fig. 5b) and CESM1-CAM5 (Fig. 5d). Several GCMs simulate dominantly negative correlations over most of the region, e.g. FGOALS-g2 (Fig. 5h) and HadGEM2-ES (Fig. 5l) while several GCMs simulate a larger area with positive correlation, e.g. IPSL-CM5A-MR (Fig. 5m) and MRI-CGCM3 (Fig. 5p).

These differences are caused by the simulated positive geopotential height centers over northwestern America being located too far to the north in the simulations (Fig. 2). Some models simulate significant negative correlations over the whole domain, because the magnitude of the negative center over the southeastern US is larger than in the observations and the center extends too far north, which make troughs deeper, so that polar air more easily invades the eastern US [e.g. CESM1-WACCM (Fig. 6e), CNRM-CM5 (Fig. 6f), FGOALS-g2 (Fig. 6h), HadGEM2-ES (Fig. 6l), and MPI-ESM-LR (Fig. 6n)].

For the relationships between the observed PNA index and winter precipitation, the observations show that the PNA index has positive correlations with precipitation over the western part of the region and along the coast, and significant negative correlations over the Ohio Valley (Fig. 6a). The mechanisms behind this pattern are that the anticyclonic circulation over the southeastern US blocks the moisture transport from the Gulf of Mexico to the Ohio Valley (Ning and Bradley 2014). Most GCMs can reproduce this spatial pattern with three different correlation centers, except for GFDL-CM3 (Fig. 6i), IPSL-CM5A-MR (Fig. 6m) and MRI-CGCM3 (Fig. 6p). This indicates that most GCMs can capture the influence of the PNA on water vapor transport, although the locations and magnitudes may be slightly different due to the northern displacement of the negative geopotential height centers over the southeastern US

3.3 Future NAO/PNA changes and relationships with regional climate

In this section, the future changes of NAO and PNA locations and magnitudes with respect to the historical model simulations, the corresponding uncertainties of these changes, and the changes of relationships between NAO/PNA and regional climate over the eastern US are examined. The future SLP and H500 anomalies are first calculated relative to the average of the period 2050–2099 for the EOF analysis. The locations and magnitudes of the NAO and PNA centers are defined as the average locations and magnitudes over the 50 grid points (~2.5 %) in the middle of the centers of the spatial regression patterns after regridding to the same 2° × 2° resolution. Then, to keep the paper concise, correlations with winter temperature under RCP4.5 scenario are selected as examples to analyze the relationships between NAO/PNA changes and the correlation pattern changes, since the correlations of temperature (Figs. 10, 11) are more uniform than precipitation (Figs. S8 & S9), and similar conclusions can be obtained from RCP2.6 and RCP8.5 scenarios.

In the future period 2050–2099, under all three scenarios (RCP2.6, 4.5, and 8.5), GCMs still simulate the NAO

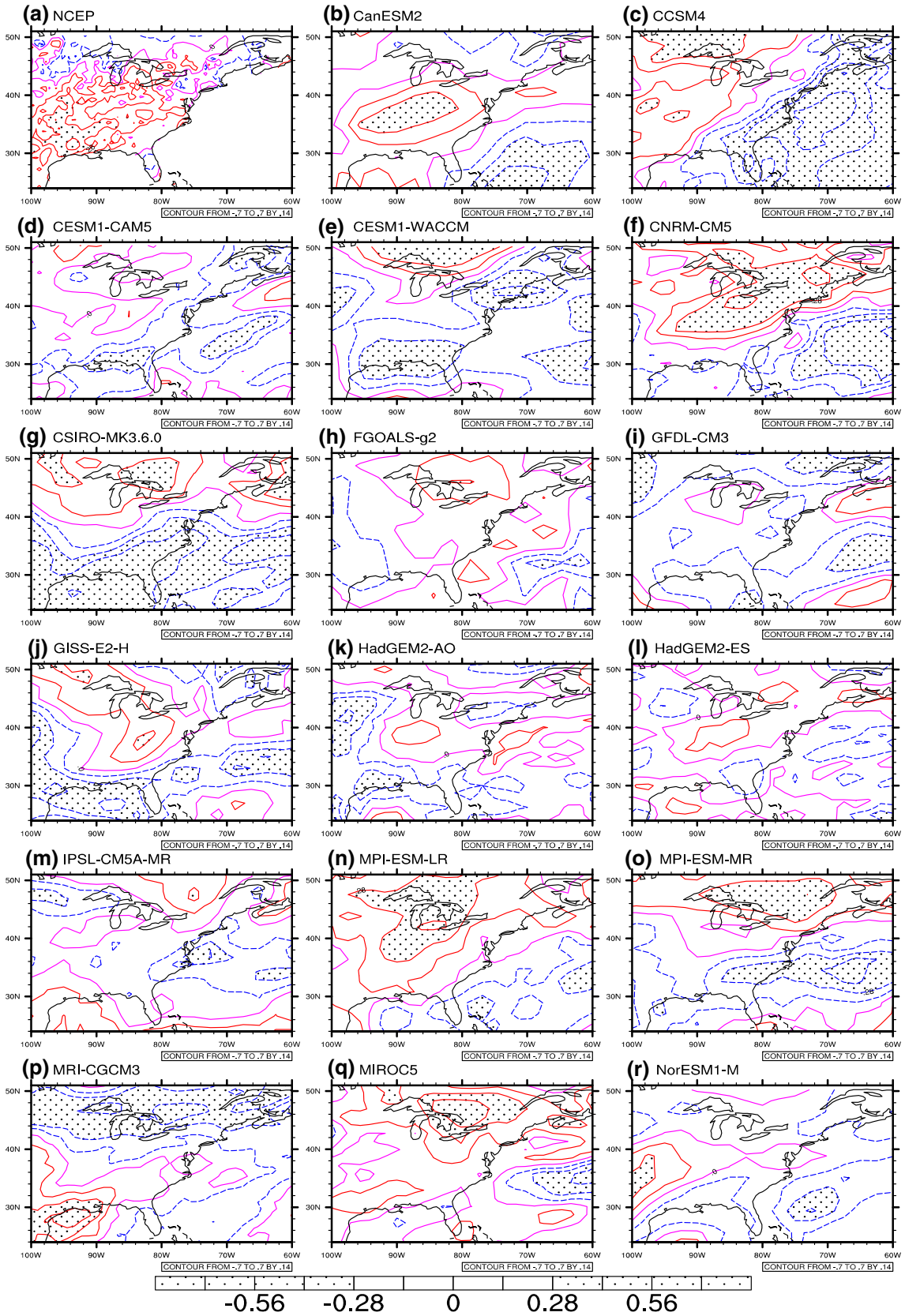

Fig. 4 The observed and GCM simulated correlations between the NAO and regional winter precipitation over the eastern US (contour interval 0.14)

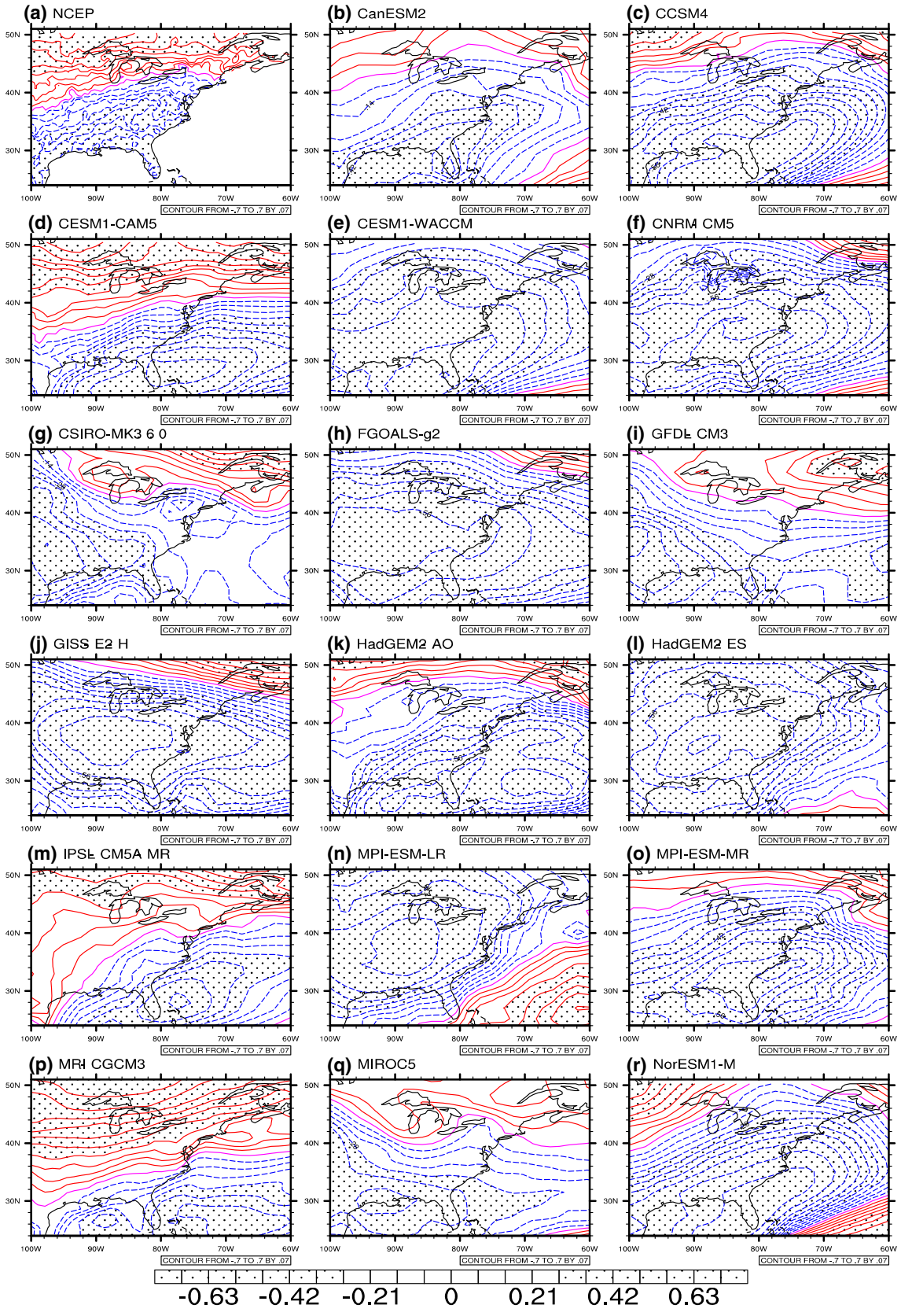

Fig. 5 The observed and GCM simulated correlations between the PNA and regional winter temperature over the eastern US (contour interval 0.07)

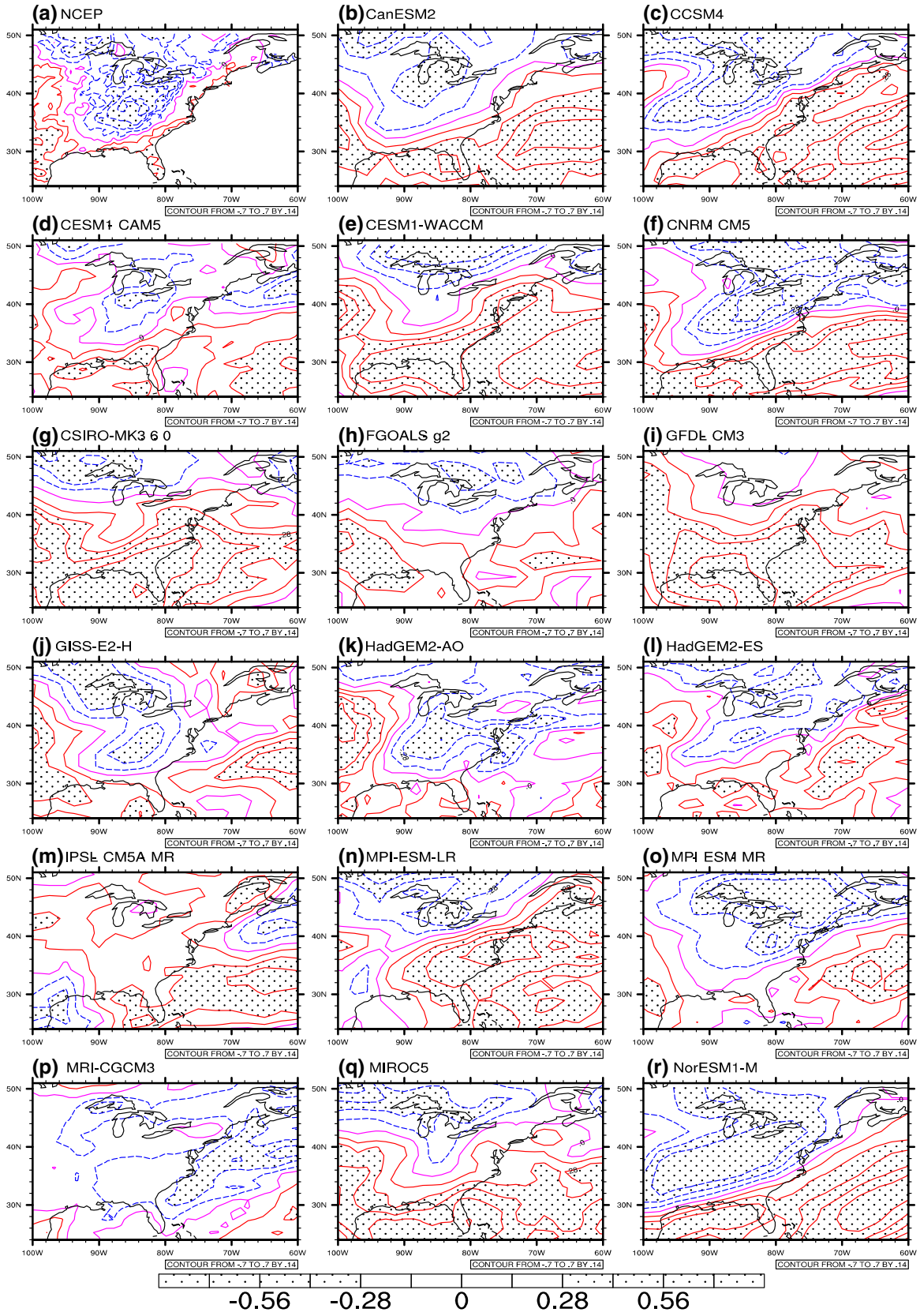

Fig. 6 The observed and GCM simulated correlations between the PNA and regional winter precipitation over the eastern US (contour interval 0.14)

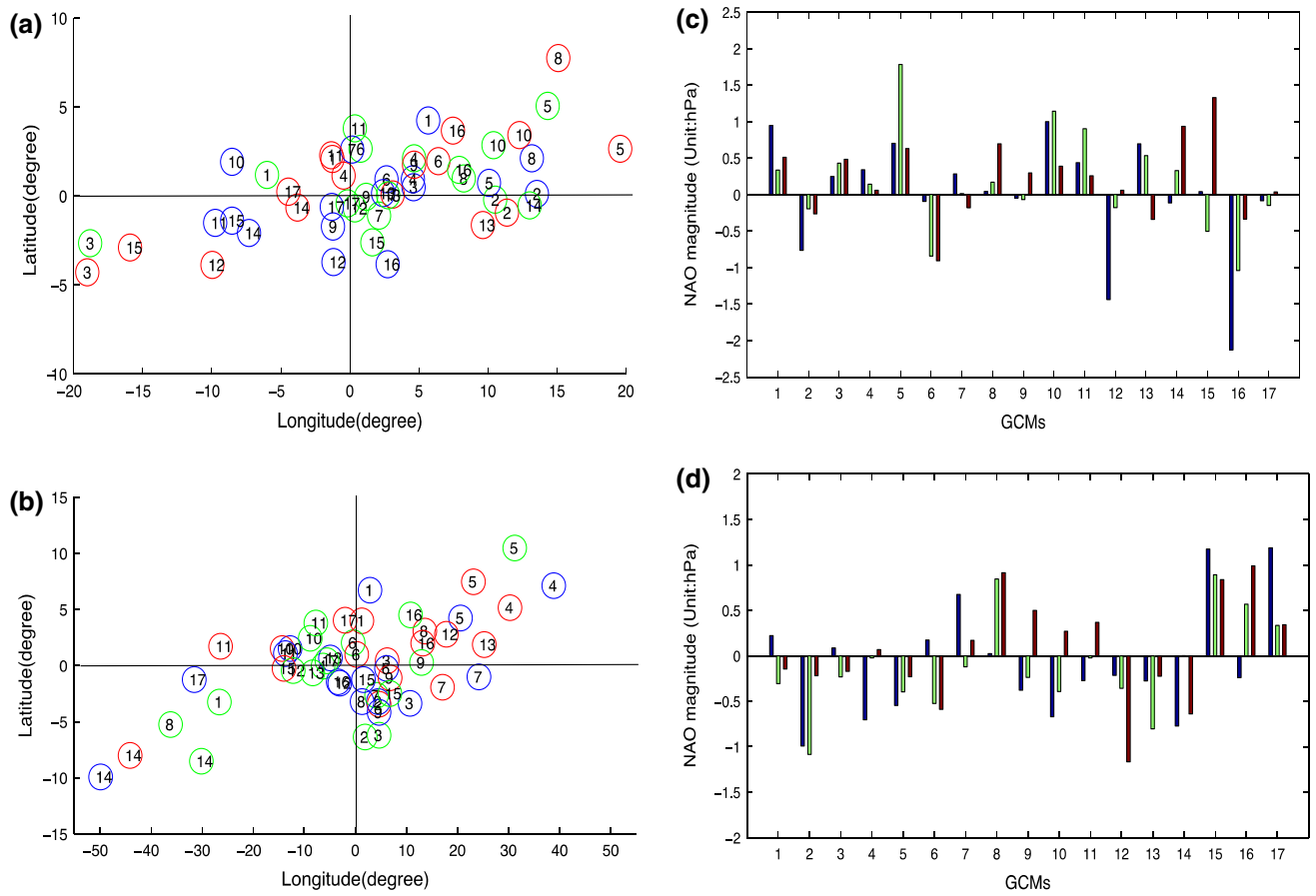

Fig. 7 Future changes of locations (**a**, **b**) and magnitudes (**c**, **d**) of NAO centers located over the Azores (**a**, **c**), and Iceland (**b**, **d**) under the RCP2.6 (*blue*), RCP4.5 (*green*), and RCP8.5 (*red*) scenarios. *1* CanESM2, *2* CCSM4, *3* CESM1-CAM5, *4* CESM1-WACCM, *5* CNRM-CM5, *6* CSIRO-Mk3.6.0, *7* FGOALS-g2, *8* GFDL-CM3, *9* GISS-E2-H, *10* HadGEM2-AO, *11* HadGEM2-ES, *12* IPSL-CM5A-MR, *13* MPI-ESM-LR, *14* MPI-ESM-MR, *15* MRI-CGCM3, *16* MIROC5, *17* NorESM1-M

and PNA as dominant low-frequency circulation patterns based on EOF analysis (c.f. Figs. S2-S7), but their locations and magnitudes change (summarized in Figs. 7, 8, 9). For the NAO Azores center (NAO center 1), under the RCP2.6 scenario, the range of longitude changes is ±10°, and this increases to −20° to +15° for RCP4.5 scenario and ±20° for RCP8.5 scenario, but with most latitude changes within ±5° (Fig. 7a). For the NAO Iceland center (NAO center 2), the ranges of longitude changes are consistent within −50° to +40° (most within ±20°) under all three scenarios, and the ranges of latitude changes are within ±10° under all three scenarios (Fig. 7b). That there is no consensus on the location changes of NAO centers among the GCMs under future warming scenarios, confirms the results from previous studies using different GCMs (e.g. Campbell et al. 1995; Huth 1997; Hu and Wu 2004), indicating these changes are associated with the different GCM responses to warming on simulating changes of NAO interannual variability and mean state (Hu and Wu 2004).

Based on the results of IPCC AR4 (IPCC 2007), in the future, there will be a SLP decrease over the Arctic region and a SLP increase over the Azores region due to the extratropical response to increased tropical sea surface temperature and an enhanced polar stratospheric vortex (Hu and Wu 2004). In the CMIP5 models that we examined, 10/17 GCMs predict an intensified Azores High under both RCP2.6 and RCP4.5 scenarios (although the GCMs are slightly different), and this number increases to 12/17 under the RCP8.5 scenario (Fig. 7c). For the Iceland center, 10/17 and 12/17 GCMs predict an intensified Icelandic low under RCP2.6 and RCP4.5 scenarios, but this number decreases to 8/17 under the RCP8.5 scenario.

When considering the two centers together, the total NAO changes are defined as:

$$\Delta\mathrm{NAO} = \Delta\mathrm{slp}_1 - \Delta\mathrm{slp}_2 \quad (1)$$

NAO increases were found in 10/17 GCMs for RCP2.6 scenario, 12/17 for RCP4.5 but only 7/17 for RCP8.5 (Fig. 9a) due to fewer GCMs simulating an intensified

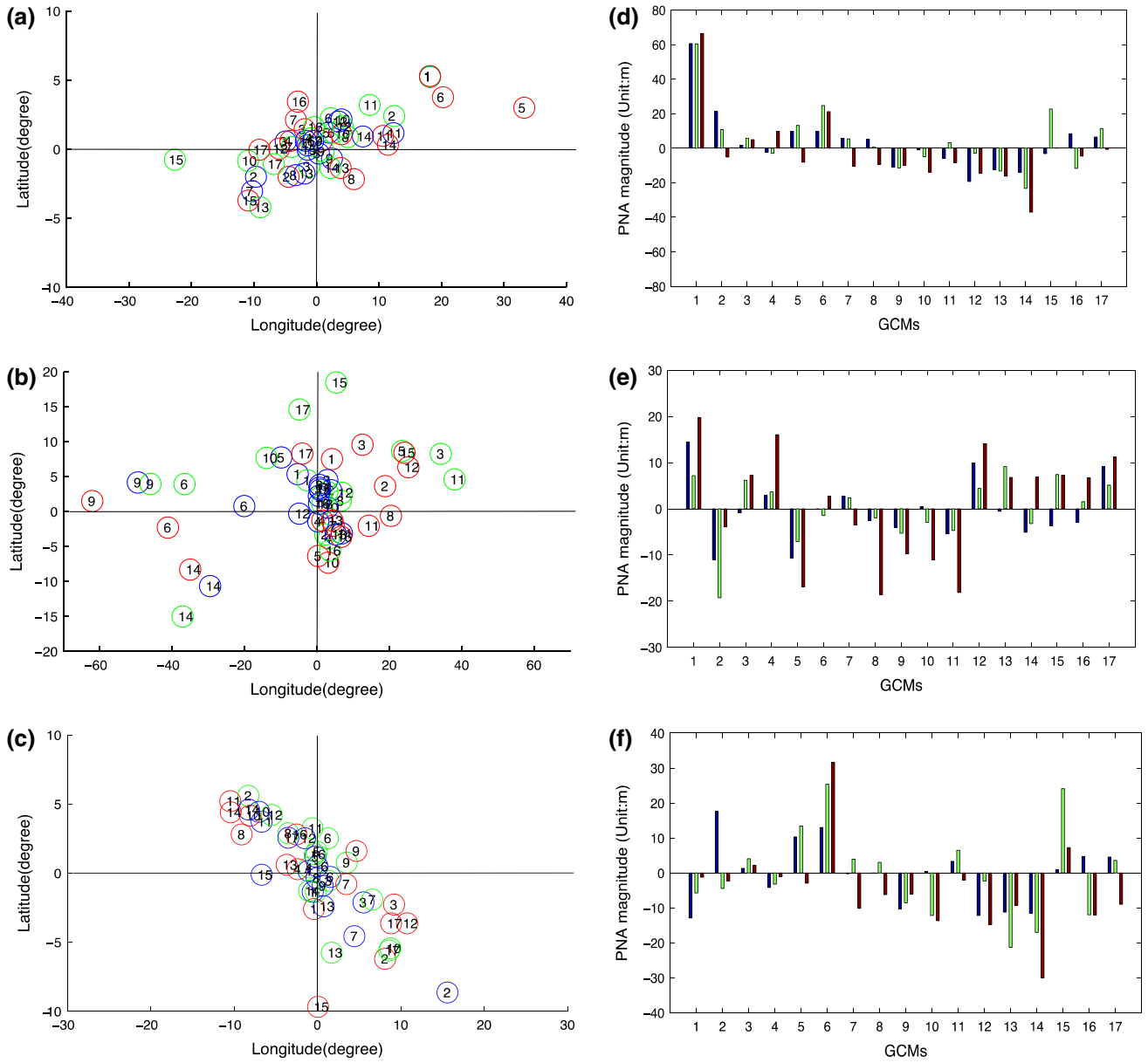

Fig. 8 Future changes of locations (**a**, **b**, **c**) and magnitudes (**d**, **e**, **f**) of PNA centers located over Aleutian Islands (**a**, **d**), northwestern North America (**b**, **e**), and the southeastern US (**c**, **f**) under the RCP2.6 (*blue*), RCP4.5 (*green*), and RCP8.5 (*red*) scenarios

Icelandic low (although the decreases are really small with only one exceeding −0.5 hPa).

Comparing the three major uncertainties, i.e. the uncertainties due to internal variability, model response and emission scenarios (Hawkins and Sutton 2009), for the location changes of NAO centers, the inter-GCM uncertainties (defined as the spread of the changes among GCMs under the same scenario) account for a large part of the total uncertainties. The total range of uncertainties increase with emission scenarios, with the magnitude changes due to increased forcing on a single GCM comparable to, or even larger than, the inter-GCM uncertainties, especially for the RCP8.5 scenario.

The factors influencing NAO relationships with winter temperature, based on the discussion in Sect. 3.2 are chosen in this analysis (i.e. total NAO magnitudes, and magnitude and longitude of the NAO center over the Azores Islands). In the future, 12/17 GCMs predict a larger area with a significant positive correlation between simulated NAO and winter temperature (Fig. 10), compared with the historical simulations (Fig. 3). 12/17 Predicted extensions/shrinkages of area with significant positive correlation, are consistent

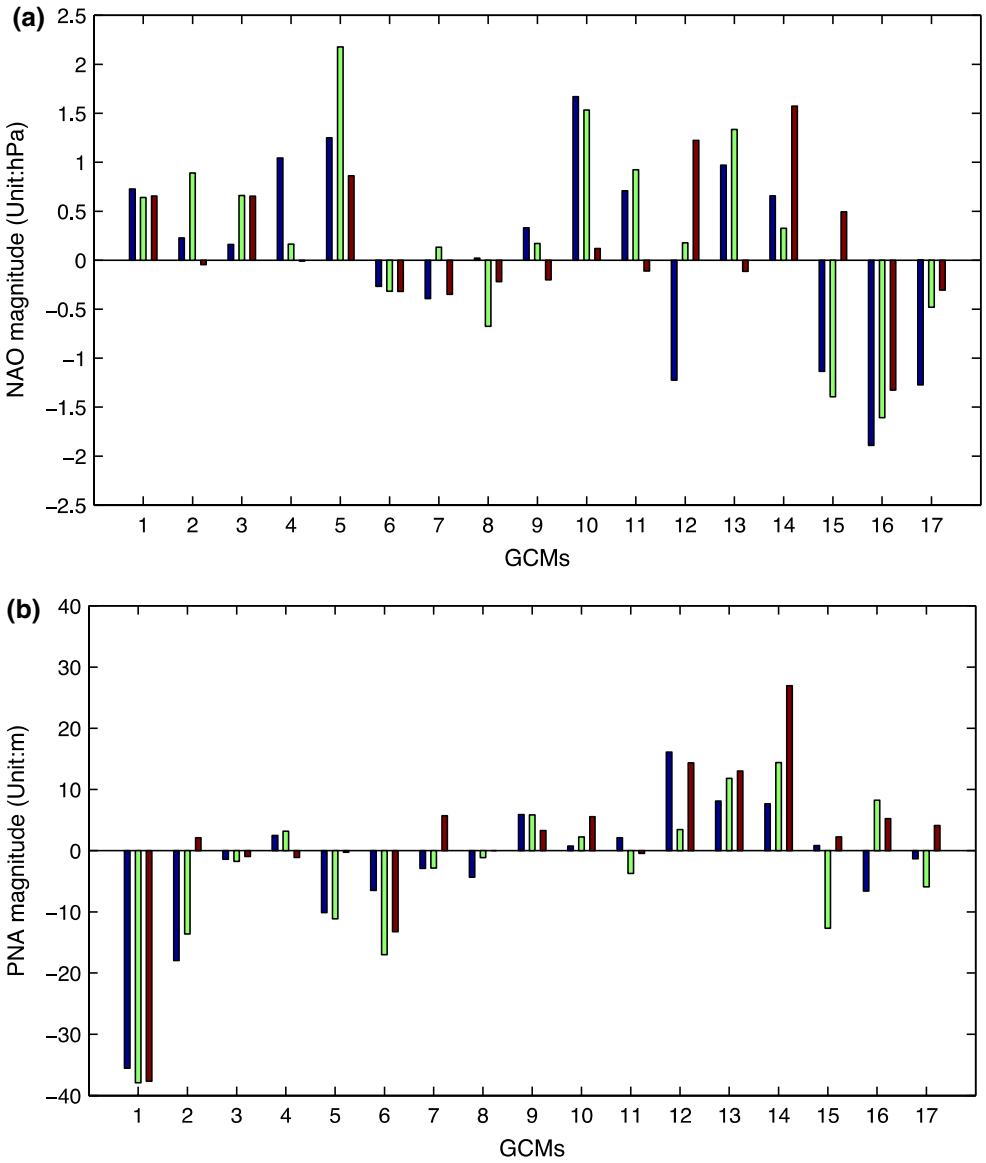

Fig. 9 Future changes of NAO (**a**) and PNA (**b**) indices under the RCP2.6 (*blue*), RCP4.5 (*green*), and RCP8.5 (*red*) scenarios

with changes of the NAO magnitudes based on the relation discussed in previous section, while more changes (13/17) are consistent with the changes of magnitude in the center over the Azores. This indicates that the correlations are highly determined by the eastern US trough magnitude, influenced by the SLP anomalies of the Azores High.

For the other factor influencing the correlation pattern, the location of the center over the Azores, only 8/17 east/west shifts of locations are consistent with the changes. Notably, for 2/3 GCMs, i.e. MPI-ESM-MR and NorESM1-M, for which none of the magnitudes of the NAO, and NAO center over the Azores are consistent with the correlation change (c.f. Figs. 3o, f, 10o, f), the shifts of the center are consistent with the correlation changes (c.f. Figs. 1o, f, S2o&f). This means the eastern/western shift of the trough brought by the location changes contribute less to the correlation changes.

For the PNA centers over the Aleutian Islands (PNA center 1), and the southeastern US (PNA center 3) most location changes are within $\pm 10°$ for longitude and $\pm 5°$ for latitude, with only a few exceptions, generally under RCP4.5 and RCP8.5 scenarios (Fig. 8a, c). However, the location changes of the center over northwestern North America (PNA center 2) are much larger ($-60°$ to $+40°$ for longitude and $-15°$ to $+20°$ for latitude, Fig. 8b); GCMs show poor performances in simulating the observed location of this center, indicating lower confidence for this change. As with the NAO, the GCMs do not show

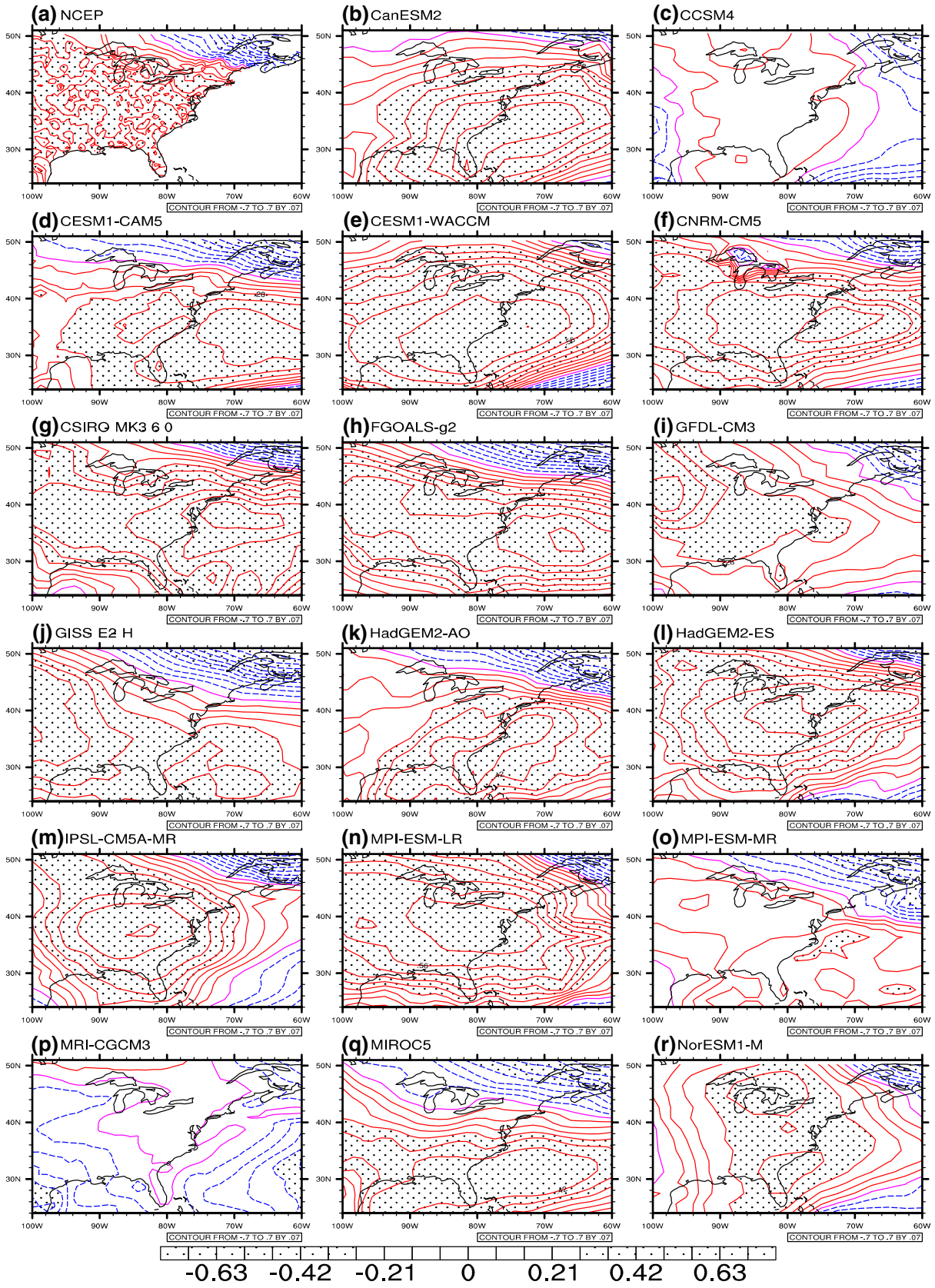

Fig. 10 The GCM simulated correlations between the NAO and regional winter temperature over the eastern US (contour interval 0.07) under the RCP4.5 scenario. The observed pattern is also shown in **a** as comparison. *Stippling* indicates correlations significant at the $p = 0.05$ level

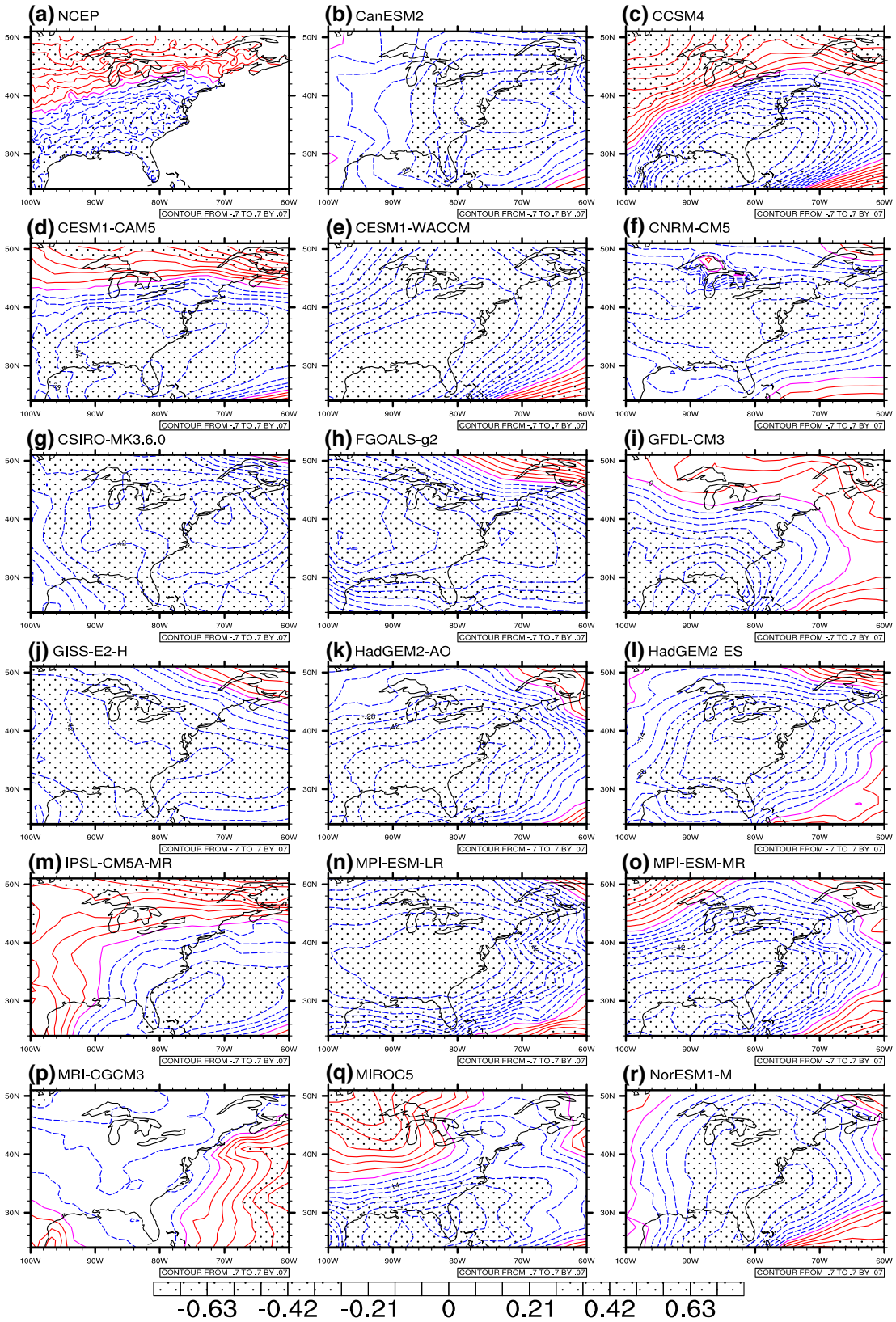

Fig. 11 Similar to Fig. 10, but for PNA

consistent location changes of the PNA centers, similar to the conclusions of previous studies (Allan 2013; Allan et al. 2014; Zhou et al. 2014), indicating that these changes are associated with different GCM responses to warming on simulating changes of variability and mean state of the future H500 wave field.

For the center magnitude changes over the Aleutian Islands, about half of the GCMs (8/17) predict decreases under the RCP2.6 and RCP4.5 scenarios, and under RCP8.5 scenario, most GCMs (12/17) predict decreases. The intensification of the Aleutian Low under future warming is consistent with previous studies (Raible et al. 2005; Meehl et al. 2006), and is related to Rossby wave propagation, which requires tropical vortex stretching due to enhanced convection in the near-equatorial Pacific (Vavrus et al. 2006). The corresponding circulation changes also induce increases of the center over northwestern North America (7/17, 9/17, and 10/17 GCMs under three scenarios) and decreases of the center over the southeastern US (8/17, 9/17, and 13/17 GCMs under three scenarios).

When considering the three centers together, the total PNA changes are defined as:

$$\Delta \mathrm{PNA} = \frac{1}{3}[-\Delta z_1 + \Delta z_2 - \Delta z_3] \quad (2)$$

Under RCP2.6 and RCP4.5 scenarios, about half of GCMs (8/17 and 7/17) predict PNA increases, while this number increases to 11/17 under RCP8.5 scenario.

GCMs show greater agreement on magnitude changes over several centers (i.e. NAO Azores center, PNA Aleutian center, and PNA center over the southeastern US) than the other two centers (i.e. NAO Iceland center and PNA center over northwestern North America) in all three scenarios, and this leads to a lower consensus on total NAO and PNA magnitude changes. This implies that it is important to investigate the future magnitude changes of individual NAO and PNA centers besides the total NAO and PNA magnitude changes.

For the location changes of PNA centers, the inter-GCM uncertainties are the major sources of the total uncertainties. The spread of location changes is usually larger under the RCP4.5 and RCP8.5 scenarios, indicating larger uncertainties under higher emission scenarios. For the magnitude changes, the uncertainties due to different scenarios for a single GCM are still smaller than the inter-GCM uncertainties, and the total uncertainties usually increase with emission scenarios, with the largest spreads under the RCP8.5 scenario.

The factors influencing PNA relationships with winter temperature chosen here are total PNA magnitude, magnitude and longitude of the PNA center over northwestern North America, and magnitude and latitude of the PNA center over the southeastern US For the PNA and temperature correlation, 9/17 GCMs predict increases in the area of the region with a significant negative correlation between winter temperature and the PNA index (Fig. 11). Based on the correlations discussed in Sect. 3.2, magnitude changes of total PNA and the PNA center over the southeastern US, are consistent with 11 correlation changes, most of which (9/11) are identical. For the PNA center over northwestern North America, the changes of magnitude are consistent with 9 correlation changes, while the longitude changes are consistent with 12 correlation changes, indicating a more important influence from the location than the magnitude. However, the changes in the latitude of the center over the southeastern US are only consistent with 6/17 correlation changes. This indicates that the changes of PNA magnitude, the longitude of the PNA center over northwestern North America, and the magnitude of the PNA center over the southeastern US strongly influence the area invaded by polar cold area, by influencing the location and magnitude of the trough over the eastern US.

4 Conclusions

17 GCMs used in CMIP5 were analyzed for their ability to simulate the spatial patterns of two important modes of large-scale climate variability—the NAO and PNA, and their influences over the eastern US The regression patterns of the first EOF modes of SLP and H500 fields were used to define the NAO and PNA. In comparisons with the results from NCEP data, the spatial patterns of the NAO and PNA are reproduced by all the GCMs, with some differences in the locations and magnitudes, indicating the GCMs are able to reasonably represent the atmospheric circulation associated with the NAO and PNA.

Most GCMs can reproduce the significant positive correlation that has been observed between NAO and winter average temperature over the eastern US NAO has a positive correlation with winter precipitation over the southern part of this region and some slight negative correlations over the northern part, but this correlation pattern is generally not significant, and is not reproduced in most GCMs. PNA has a positive correlation with winter temperature over the northwest and a negative correlation over the southeastern US All GCMs can reproduce this pattern, but several GCMs simulate a negative correlation over almost the entire region due to the differences between observed and simulated positive geopotential height centers over northwestern America and southeastern US For winter precipitation, PNA has a positive correlation over the western part, a negative correlation over the Ohio Valley, and a slight positive correlation over the coastal region; most GCMs can reproduce this pattern, though with some displacements. Differences between the observed and

GCM-simulated relationships result from differences in the simulated magnitudes and locations of the geopotential height centers.

The differences of the correlation patterns indicate that although the GCMs can reasonably reproduce the two patterns of large-scale climate variability, on the regional scale, GCMs have some deficiencies in reproducing the detailed relationships because of the limited abilities of GCMs to reproduce the background dynamics, e.g. stationary waves and jet streams (Lee and Black 2013; Davini and Cagnazzo 2014). These differences from the observed and simulated relationships should be taken into consideration, and bias-corrections should be applied before application to downscaling methods, to generate high-resolution regional climate data.

In the future period 2050–2099, the projected NAO and PNA changes in magnitudes and locations show large inter-GCM uncertainties, as well as uncertainties related to scenarios. Usually, the uncertainties in the location changes of individual centers and total NAO magnitude changes are due to both model response and emission scenarios, while, the uncertainties in the magnitude changes of total PNA and individual centers are mainly from model responses. Moreover, GCMs show higher agreements on magnitude changes over individual centers than for the total NAO and PNA magnitude changes. The winter temperature correlation changes over the eastern US are usually highly influenced by changes in the magnitude of the NAO center over the Azores, and changes of total NAO magnitude, as well as by changes in the longitude of the PNA center over northwestern North America, changes in total PNA magnitude, and the change in magnitude of the PNA center over the southeastern US These results imply that in future mechanism investigations, it is important to consider the influences of both the location and magnitude changes of individual NAO and PNA centers, in addition to the total NAO and PNA magnitude changes.

Based on the findings of this study, when applying the changes of the two teleconnections to future downscaling, temperature can be downscaled with more confidence than precipitation over the eastern US Considering the GCMs' deficiencies in reproducing the locations of the PNA center over northwestern North American and the magnitude of the NAO center over the Azores, bias-correction should be applied before the downscaling procedure. Moreover, to reduce the inter-GCM uncertainties, methods like multi-model ensemble averaging should be also applied, with weights based on the GCMs' performances in reproducing the historical correlations with surface climate over the eastern US.

Acknowledgments This research is jointly supported by the US Department of the Interior's Northeast Climate Science Center, under USGS funding G12AC00001, the Strategic and Special Frontier Project of Science and Technology of the Chinese Academy of Sciences (Grant No. XDA05080800), the National Natural Science Foundation of China (Grant No. 41420104002) and The Priority Academic Development Program of Jiangsu Higher Education Institutions (Grant No. 164320H116). The high-resolution observation data were obtained from the Climatic Research Unit at University of East Anglia. The NCEP reanalysis data were obtained from the National Oceanic and Atmospheric Administration (NOAA) Earth System Research Laboratory (ESRL)—Physical Science Division (PSD). The WCRP CMIP5 multi-model dataset is made available by the Program for Climate Model Diagnosis and Intercomparison (PCMDI) and the WCRP's Working Group on Coupled Modeling (WGCM). James Hurrell kindly provided the observed NAO time series. The observed PNA time series were obtained from National Oceanic and Atmospheric Administration (NOAA) Climate Prediction Center (CPC). We would like to acknowledge high-performance computing support from Yellowstone (ark:/85065/d7wd3xhc) provided by NCAR's Computational and Information Systems Laboratory, sponsored by the National Science Foundation. We thank referees for their valuable comments, which greatly improved the manuscript.

References

Allan AM (2013) Analyzing the present and future Pacific-North American teleconnection using global and regional climate models. Doctoral dissertation, Oregon State University, p 190

Allan AM, Hostetler SW, Alder JR (2014) Analysis of the present and future winter Pacific-North American teleconnection in the ECHAM5 global and RegCM3 regional climate models. Clim Dyn 42:1671–1682. doi:10.1007/s00382-013-1910-x

Bai X, Wang J, Sellinger C, Clites A, Assel R (2012) Interannual variability of Great Lakes ice cover and its relationship to NAO and ENSO. J Geophys Res 117:C03002. doi:10.1029/2010JC006932

Barnston AG, Livezey RE (1987) Classification, seasonality, and persistence of low-frequency atmospheric circulation patterns. Mon Weather Rev 115:1083–1126

Bellouin N, Boucher O, Haywood J, Johnson C, Jones A, Rae J, Woodward S (2007) Improved representation of aerosols for HadGEM2. Meteorological Office Hadley Centre, Technical Note 73, March 2007

Bentsen M et al (2012) The Norwegian earth system model, NorESM1-M—part 1: description and basic evaluation. Geosci Model Dev Discuss 5:2843–2931

Bradbury JA, Keim BD, Wake CP (2003) The influence of regional storm tracking and teleconnections on winter precipitation in the Northeastern United States. Ann Assoc Am Geogr 93:544–556

Campbell GG, Kittel TGF, Meehl GA, Washington WM (1995) Low-frequency variability and CO2 transient climate change. Part 2: EOF analysis of CO2 and model-configuration sensitivity. Glob Planet Change 10:201–216

Casado MJ, Pastor MA (2012) Use of variability modes to evaluate AR4 climate models over the Euro-Atlantic region. Clim Dyn 38:225–237

Chylek P, Li J, Dubey MK, Wang M, Lesins G (2011) Observed and model simulated 20th century Arctic temperature variability: Canadian earth system model CanESM2. Atmos Chem Phys Discuss 11:22893–22907

Coleman JSM, Rogers JC (2003) Ohio River Valley winter moisture conditions associated with the Pacific-North American teleconnection pattern. J Clim 16:969–981

Collins WJ et al (2008) Evaluation of the HadGEM2 model. Meteorological Office Hadley Centre, Technical Note 74, Nov 2008

Davini P, Cagnazzo C (2014) On the misinterpretation of the North Atlantic Oscillation in CMIP5 models. Clim Dyn 43:1497–1511. doi:10.1007/s00382-013-1970-s

Donner LJ et al (2011) The dynamical core, physical parameterizations, and basic simulation characteristics of the atmospheric component AM3 of the GFDL Global Coupled Model CM3. J Clim 24:3484–3519

Ge Y, Gong G, Frei A (2009) Physical mechanisms linking the winter Pacific-North American teleconnection pattern to spring North American snow depth. J Clim 22:5135–5148

Gent PR et al (2011) The community climate system model version 4. J Clim 24:4973–4991

Handorf D, Dethloff K (2012) How well do state-of-the-art atmosphere–ocean general circulation models reproduce atmospheric teleconnection patterns? Tellus A 64:19777. doi:10.3402/tellusa.v64i0.19777

Hannachi A (2007) Pattern hunting in climate: a new method for finding trends in gridded climate data. Int J Climatol 27:1–15

Harris I, Jones PD, Osborn TJ, Lister DH (2014) Updated high-resolution grids of monthly climatic observations—the CRU TS3.10 Dataset. Int J Climatol 34:623–642

Hartley S, Keables MJ (1998) Synoptic associations of winter climate and snowfall variability in New England, USA, 1950–1992. Int J Climatol 18:281–298

Hartmann DL, Klein Tank AMG, Rusticucci M, Alexander LV, Brönnimann S, Charabi Y, Dentener FJ, Dlugokencky EJ, Easterling DR, Kaplan A, Soden BJ, Thorne PW, Wild M, Zhai PM (2013) Observations: atmosphere and surface. In: Stocker TF, Qin D, Plattner G-K, Tignor M, Allen SK, Boschung J, Nauels A, Xia Y, Bex V, Midgley PM (eds) Climate change 2013: the physical science basis. Contribution of Working Group I to the Fifth Assessment Report of the Intergovernmental Panel on Climate Change. Cambridge University Press, Cambridge

Hawkins E, Sutton R (2009) The potential to narrow uncertainty in regional climate predictions. Bull Am Meteorol Soc 90:1095–1107

Hewitson BC, Crane RG (1996) Climate downscaling: techniques and application. Clim Res 7:85–95

Hewitson BC, Crane RG (2006) Consensus between GCM climate change projections with empirical downscaling: precipitation downscaling over South Africa. Int J Climatol 26:1315–1337

Hollingsworth A, Arpe K, Tiedtke M, Capaldo M, Savuärvi H (1980) The performance of a medium-range forecast model in winter—impact of physical parameterizations. Mon Weather Rev 108:1736–1773

Horton RG, Eastering W, Kates R, Ruth M, Sussman E, Whelchel A, Wolfe D, Lipschultz F (2014) Ch. 16: Northeast. Climate change impacts in the United States: the third national climate assessment. Melillo JM, Terese (T.C.) Richmond, Yohe GW (eds) US Global Change Research Program, 371–395. doi:10.7930/JOSF2T3P

Hu Z-Z, Wu Z (2004) The intensification and shift of the annual North Atlantic oscillation in a global warming scenario simulation. Tellus 56A:112–124

Hurrell JW (1995) Decadal trends in the North Atlantic oscillation: regional temperature and precipitation. Science 269:676–679

Hurrell JW, Deser C (2009) North Atlantic climate variability: the role of the North Atlantic oscillation. J Mar Syst 78:28–41

Hurrell JW, National Center for Atmospheric Research Staff (eds) (2013) The climate data guide: Hurrell North Atlantic oscillation (NAO) Index (station-based). Last modified 08 Oct 2013. Retrieved from https://climatedataguide.ucar.edu/climate-data/hurrell-north-atlantic-oscillation-nao-index-station-based

Huth R (1997) Continental-scale circulation in the UKHI GCM. J Clim 10:1545–1561

IPCC (2007) Climate Change: the physical science basis. Cambridge University Press, Cambridge, UK and New York, NY, USA

Johns TC et al (2006) The new Hadley Centre climate model (HadGEM1): evaluation of coupled simulations. J Clim 19:1327–1353

Kalnay E, Kanamitsu M, Kistler R, Collins W, Deaven D, Gandin L, Iredell M, Saha S, White G, Woollen J (1996) The NCEP/NCAR 40-year reanalysis project. Bull Am Meteorol Soc 77:437–471

Kunkel KE et al. (2013) Monitoring and understanding trends in extreme storms: state of knowledge. Bull Am Meteorol Soc 94:499–514

Kunkel KE, Angel JR (1999) Relationship of ENSO to snowfall and related cyclone activity in the contiguous United States. J Geophys Res 104:19425–19434. doi:10.1029/1999JD900010

Leathers DJ, Yarnal B, Palecki MA (1991) The Pacific/North American teleconnection pattern and United States climate. Part I: regional temperature and precipitation associations. J Clim 4:517–528

Lee Y-Y, Black RX (2013) Boreal winter low-frequency variability in CMIP5 models. J Geophys Res Atmos 118:6891–6904. doi:10.1002/jgrd.50493

Lian T, Chen D (2012) An evaluation of rotated EOF analysis and its application to tropical Pacific SST variability. J Clim 25:5361–5373

Liu H-L et al (2010) Thermosphere extension of the whole atmosphere community climate model. J Geophys Res. doi:10.1029/2010JA015586

Marsland SJ, Haak H, Jungclaus JH, Latif M, Röske F (2003) The Max-Planck-Institute global ocean/sea ice model with orthogonal curvilinear coordinates. Ocean Model 5:91–127

Meehl GA, Teng H, Branstator G (2006) Future changes of El Niño in two global coupled climate models. Clim Dyn 26:549–566. doi:10.1007/s00382-005-0098-0

Meehl GA et al (2007) Global climate projections. In: Solomon S et al (eds) Climate change 2007: the physical science basis. Cambridge University Press, Cambridge, pp 747–845

Mignot J, Bony S (2013) Presentation and analysis of the IPSL and CNRM climate models used in CMIP5. Clim Dyn. doi:10.1007/s00382-01301720-1

Moss RH et al (2010) The next generation of scenarios for climate change research and assessment. Nature 463:747–756

Neale RB, Richter J, Park S, Lauritzen PH, Vavrus SJ, Rasch PJ, Zhang M (2013) The mean climate of the Community Atmosphere Model (CAM4) in forced SST and fully coupled experiments. J Clim 26:5150–5168

Ning L, Bradley RS (2014) Winter precipitation variability and corresponding teleconnections over the northeastern United States. J Geophys Res Atmos. doi:10.1002/2014JD021591

Ning L, Bradley RS (2015) Winter climate extremes over the northeastern United States and southeastern Canada and teleconnections with large-scale modes of climate variability. J Clim 28:2475–2493

Ning L, Qian Y (2009) Interdecadal change of extreme precipitation over South China and its mechanism. Adv Atmos Sci 26:109–118

Ning L, Mann ME, Crane R, Wagener T (2012a) Probabilistic projections of climate change for the mid-Atlantic region of the United States—validation of precipitation downscaling during the historical era. J Clim 25:509–526

Ning L, Mann ME, Crane R, Wagener T, Najjar RG, Singh R (2012b) Probabilistic projections of anthropogenic climate change impacts on precipitation for the mid-Atlantic region of the United States. J Clim 25:5273–5291

Notaro M, Wang W-C, Gong W (2006) Model and observational analysis of the northeast US regional climate and its relationship to the PNA and NAO patterns during early winter. Mon Weather Rev 134:3479–3505

Raddatz TJ, Reick CH, Knorr W, Kattge J, Roeckner E, Schnur R, Schnitzler KG, Wetzel P, Jungclaus J (2007) Will the tropical land biosphere dominate the climate–carbon cycle feedback during the twenty-first century? Clim Dyn 29:565–574

Raible CC, Stocker TF, Yoshimori M, Renold M, Beyerle U, Casty C, Luterbacher J (2005) Northern hemispheric trends of pressure indices and atmospheric circulation patterns in observation, resconstructions, and coupled GCM simulations. J Clim 18:3968–3982

Randall DA et al (2007) Climate models and their evaluation. In: Solomon S et al (eds) Climate change 2007: the physical science basis. Cambridge University Press, Cambridge, pp 589–662

Rotsayn L, Collier MA, Dix MR, Feng Y, Gordon HB, O'Farrell SP, Smith IN, Syktus J (2010) Improved simulation of Australian climate and ENSO-related climate variability in a global climate model with an interactive aerosol treatment. Int J Climatol 30(7):1067–1088

Schmidt GA et al (2014) Configuration and assessment of the GISS ModelE2 contributions to the CMIP5 archive. J Adv Model Earth Syst 6:141–184. doi:10.1002/2013MS000265

Stephenson DB, Pavan V, Collins M, Junge MM, Quadrelli R (2006) North Atlantic Oscillation response to transient greenhouse gas forcing and the impact on European winter climate: a CMIP2 multi-model assessment. Clim Dyn 27:401–420

Stoner AM, Hayhoe K, Wuebbles DJ (2009) Assessing general circulation model simulations of atmospheric teleconnection patterns. J Clim 22:4348–4372

Taylor KE, Stouffer RJ, Meehl GA (2012) An overview of CMIP5 and the experiment design. Bull Am Meteorol Soc 93:485–498

Trenberth KE et al (2007) Observations: surface and atmospheric climate change. In: Solomon S et al (eds) Climate change 2007: the physical science basis. Cambridge University Press, Cambridge, pp 235–336

Van Vuuren DP et al (2011) The representative concentration pathways: an overview. Clim Change 109:5–31

Vavrus S, Notaro M, Liu Z (2006) A mechanism for abrupt climate change associated with tropical Pacific SST. J Clim 19:242–256

Voldoire A et al (2012) The CNRM-CM5.1 global climate model: description and basic evaluation. Clim Dyn 40(9):2091–2121. doi:10.1107/s00382-01101259-y

Wallace JM, Gutzler DS (1981) Teleconnections in the geopotential height field during the Northern Hemisphere winter. Mon Weather Rev 109:784–812

Watanabe M et al (2010) Improved climate simulation by MIROC5: mean states, variability, and climate sensitivity. J Clim 23:6312–6335

Wilks DS (2006) Statistical methods in atmospheric sciences, 2nd edn. Academic Press, Burlington, p 648

Yukimoto S et al (2011) Meteorological research institute-earth system model version 1 (MRI-ESM1): model description. Technical Reports of the Meteorological Research Institute No. 64, 2011, p 83

Zhou T, Song F, Chen X (2013) Historical evolution of global and regional surface air temperature simulated by FGOALS-s2 and FGOALs-g2: How reliable are the model results? Adv Atmos Sci 30:638–657

Zhou Z-Q, Xie S-P, Zheng X-T, Liu Q, Wang H (2014) Global warming-induced change in El Niño teleconnections over the north Pacific and North America. J Clim 27:9050–9064